REPORT DOCUMENTATION PAGE

AFRL-SR-BL-TR-01-

0553

1. AGENCY USE ONLY *(Leave blank)*	2. REPORT DATE	3. REPORT TYPE AND DATES COVERED
	30Sep01	Final Report, 01Oct00 - 30Sep01

4. TITLE AND SUBTITLE
STTR Phase I Final Report

"Analysis and Design Tools for Combustion Instabilities"

5. FUNDING NUMBERS
C
F49600-00-C0056

6. AUTHOR(S)
Andrew Godfrey, Uri Vandsburger and Jeff Borggaard

7. PERFORMING ORGANIZATION NAME(S) AND ADDRESS(ES)
AeroSoft, Inc.

1872 Pratt Drive, Ste. 1275

Blacksburg, VA 24060-6363

Virginia Tech, Blacksburg, VA 24060

8. PERFORMING ORGANIZATION REPORT NUMBER

AS01-10-01

9. SPONSORING/MONITORING AGENCY NAME(S) AND ADDRESS(ES)
USAF, AFRL

AF Office of Scientific Research

801 N. Randolph St. Room 732

Arlington, VA 22203

10. SPONSORING/MONITORING AGENCY REPORT NUMBER

11. SUPPLEMENTARY NOTES
Item 0001AD

12a. DISTRIBUTION AVAILABILITY STATEMENT

Approved for public release, distribution unlimited

12b. DISTRIBUTION CODE

AIR FORCE OFFICE OF SCIENTIFIC RESEARCH (AFOSR)
NOTICE OF TRANSMITTAL DTIC. THIS TECHNICAL REPORT
HAS BEEN REVIEWED AND IS APPROVED FOR PUBLIC RELEASE
LAW AFR 190-12. DISTRIBUTION IS UNLIMITED

13. ABSTRACT *(Maximum 200 words)*

Computational analysis of flow through a model combustor is completed using several commercial CFD packages. Both global and reduced-order models prove ineffective for this gas-turbine application. These models exhibit significant stiffness or require numerical damping of product concentrations. The existence of a CH_4+M reaction is critical to the performance of any methane/air chemistry model. A 12-specie model based on a set of elementary reactions is found to perform well. The flow is made unsteady by imposing a sinusoidally varying inflow profile. The pre-mixed profile to the combustor is obtained by modeling four swirl-vane configurations in the fuel nozzle. By fitting the profiles with a Lagrange polynomial, the sensitivity to swirl-vane location can be determined. Time-frozen snap shots of the unsteady simulation are taken to compute the sensitivity to inlet velocity and the swirl-vane location. The three physical elements included in the study include three-dimensional mixing of methane and air, combustion of a pre-mixed flame and induced mass-flow unsteadiness. True unsteady sensitivities are computed in a one-dimensional context for a 10:1 Riemann problem and a quasi-1D nozzle with heat addition.

20011126 123

14. SUBJECT TERMS				15. NUMBER OF PAGES
Unsteady combustion				23
Sensitivity analysis				**16. PRICE CODE**
Methane/air chemistry				

17. SECURITY CLASSIFICATION OF REPORT	18. SECURITY CLASSIFICATION OF THIS PAGE	19. SECURITY CLASSIFICATION OF ABSTRACT	20. LIMITATION OF ABSTRACT
UNCLASSIFIED	UNCLASSIFIED	UNCLASSIFIED	UL

Standard Form 298 (Rev. 2-89) (EG)
Prescribed by ANSI Std. 239.18

STTR AF00-T019 Phase I Final Report
Contract No. F49620-00-C-0056
"ANALYSIS AND DESIGN TOOLS FOR COMBUSTION
INSTABILITIES"

Principal Investigator:
Andrew G. Godfrey
AeroSoft, Inc.
1872 Pratt Drive, Ste. 1275
Blacksburg, VA 24060

Contract Manager:
Belinda B. King
AFOSR/NM
801 N. Randolph Dr., Room 732
Arlington, VA 22203-1977

October 1, 2000 – September 30, 2001

1 Purpose of the Work

The overall goal of this project is to develop an accurate design tool for predicting and controlling unsteady oscillations in high-performance, gas-turbine combustors. The sensitivity equation method (SEM) has been developed in a stand-alone commercial package (called $\mathcal{SENSE}$) to the point of providing turbulent flow sensitivities for chemically reacting flows (and all subsets). This STTR project adds the element of *unsteadiness* which no sensitivity method exploits better than SEM. Our focus during Phase I is to develop such a tool using the $\mathcal{GASP}$ and $\mathcal{SENSE}$ CFD software to study the aero-acoustic instabilities observed in the National Energy Technology Laboratory (NETL) combustor. Ultimately this software will be useful for determining optimal placement of controllers and transducers.

1.1 Plans for Phase II

After the Phase I, we propose to begin a three-part effort in Phase II – each directed by a member of the STTR team. AeroSoft's portion will focus on developing a driver for coupling both the flow and sensitivity solvers. Much of the computational work performed in a flow solver can be re-used to compute sensitivities. These include the flow solution (of course) as well as grid area, volume and metrics, flux Jacobians, time-integration methods. For unsteady applications, the driver would be used to call $\mathcal{GASP}$ for a flow update and then pass required information for a sensitivity update. In the steady case, the driver would call $\mathcal{GASP}$ once the flow solution has converged and then pass the relevant information to $\mathcal{SENSE}$. The majority of this exchange is controlled using a Message Passing Interface (MPI). This solver coupling increases the marketability of the sensitivity software because the connection between flow and sensitivity solver is completed automatically. Currently, the user must be able to export a specific solution format and then set up input files for $\mathcal{SENSE}$. The coupling software therefore simplifies the user's workload. If a generic flow solver is selected, then software currently existing in $\mathcal{SENSE}$ would be used to compute the re-usable information.

The ICAM effort would focus on using the Ansatz from Floquet theory to construct a solution to the linear sensitivity equations for a periodic flow. We would exploit this structure for efficient computation of this class of time-varying flow sensitivity problems. Also, ICAM will work on sensitivity problems involving turbulent flows where the design variable controls the geometry. This is the biggest stumbling block in $\mathcal{SENSE}$ currently and would greatly increase the marketability of the product.

The Mechanical Engineering Department would be responsible for designing and completing an unsteady, combustion experiment of broad interest which could be simulated with the current capabilities of $\mathcal{GASP}$. Rather than request funding to increase the fidelity of $\mathcal{GASP}$ to run a specific combustion problem, we feel a more productive approach is to design a combustion problem where the focus can be placed on the sensitivity problem. The experimental geometry and results would serve as a test-bed for the driver/boundary-condition software developments given above. Also, a team member will be responsible for running an unsteady $\mathcal{GASP}/\mathcal{SENSE}$ simulation in the current uncoupled fashion to compare with the improvements provided by the coupling driver software. This comparison would occur at the end of the Phase II.

2

1.2 Elements of the Phase I

During the 12 months of the project, the following technical objectives have been accomplished:

1. We implemented a simple, yet adequate chemistry mechanism into $\mathcal{GASP}$ and $\mathcal{SENSE}$, and applied to the reacting flow within the NETL rig. With a quasi-steady flow solution, we computed the sensitivity to inlet velocity and swirler-to-injector distance.

2. Using the quasi-steady solution as a starting point, we simulated the unsteady combustion within the NETL rig. We determined the requirements to accurately simulate the unsteady oscillations induced by thermo-acoustic interaction.

3. Using time-frozen snapshots from the unsteady flow simulation, we computed sensitivities to inlet velocity and swirler location. Note that the Sensitivity-Equation Method (SEM) yields a partial differential equation for the *unsteady* sensitivity. Our goal in this STTR project is to utilize this capability, which other sensitivity methods lack.

4. We solved the one-dimensional, unsteady flow and sensitivity equations simultaneously. The initial value problem corresponds to a 10 : 1 (by pressure) Riemann problem. Also, a quasi-1D approximation is implemented to determine the sensitivity to inlet density and geometric changes.

1.3 Conclusions from the Phase I

Several levels of sophistication in chemistry modeling have been investigated including one/two-step models, reduced global models and fundamental mechanisms. We conclude that a model which uses a fundamental reaction mechanism provides the best performance both numerically and physically. We also have determined the best way to solve an internal combustion problem where no geometric flame holder exists, such as the NETL combustor. We have computed flow sensitivities to the inlet velocity and swirler-ring location. These sensitivities are most significant around the flame front. The feasibility of a time-accurate sensitivity solution is proven using a one-dimensional Riemann problem.

2   Brief Description of the Work Carried Out

Our Phase I goal is to simulate a forced instability in a simplified version of the NETL combustor. A baseline pre-mixed profile is imposed as a planar jet into the combustion region. This profile is determined by solving the steady-state, axi-symmetric flow equations for the fuel nozzle alone. To determine the sensitivity profile, we assume the mass-fraction profiles can be approximated using a cubic Lagrange polynomial in the swirler location. Turbulent mixing of air and methane in the nozzle occurs via a two-equation model. The baseline profile is made unsteady via a time-dependent sinusoidal function where the amplitude and frequency are deduced from experimental data.

The flow in the combustor uses a finite-rate approximation with twelve reacting species. The steady-state solution serves as the starting point (*i.e.*, $t = 0$) for the time-dependent calculation. At several points in time, the flow variables are output and a sensitivity calculation is performed. While this is not a true unsteady sensitivity, we have established the best chemistry model, included the most important physics in the study and gained sensitivity insight. A true unsteady sensitivity solution has been completed by solving a one-dimensional Riemann problem and a quasi-1D problem.

3   Results

3.1   The Design Problem

Four different swirler configurations are available in the fuel-nozzle section of the NETL gas-turbine combustor. In particular, the swirl vanes can be placed farther upstream of the fuel-spoke injector in increments as shown in Fig. 1. The first case corresponds to locating the swirl vanes 3.25" upstream of the combustor. Each successive case corresponds to the vanes being located one inch farther upstream (*i.e.*, to the left). One of our design variables is this swirler location.

Under the calendar and financial constraints of a Phase I effort, we seek to simulate a chemically reacting flow which captures the important physics of the gas-turbine combustor while excluding more complicated features such as a self-excited flow instability and three-dimensional effects. Our goal is not to model the entire NETL rig, but to identify the relevant aspects of the flow and then, investigate the sensitivity to the swirler's location. We believe that these important features include (1) swirling fuel/air mixing in the fuel nozzle, (2) turbulent combustion of a pre-mixed flame in the combustor, and (3) induced unsteady mass flow which leads to an unsteady fuel-to-air equivalence ratio.

For computational simplicity, we approximate the three-dimensional full NETL configuration with a two-dimensional version which begins at the nozzle exit and extends to the end of the refractory plug. After trying several simplified methane-air chemistry models including one/two-step mechanisms [1] and reduced global models [2, 3], we resort to a more fundamental reaction mechanism [4] which contains 12 species and 32 elementary reactions (including collision-partner reactions separately). After testing, the one/two-step mechanisms performed with extreme stiffness. Increasingly small time steps failed to yield a reasonable solution. The complexity of the Paczko/Peters reduced models justified using numerical source Jacobians rather than tediously deriving analytical ones. This added to the computational cost per iteration and required major modifications to the sensitivity software.
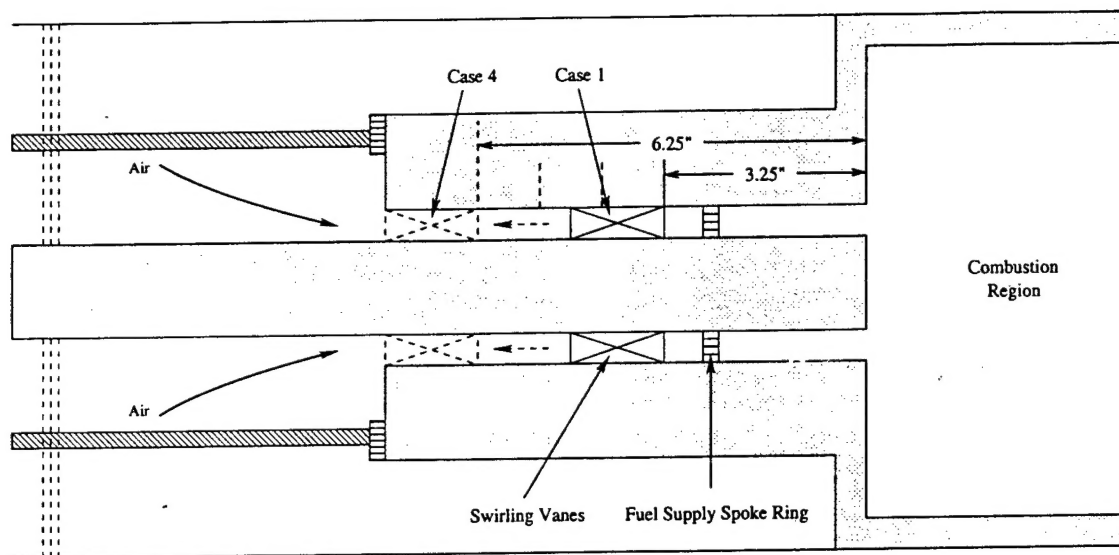
4

Figure 1: Fuel nozzle showing the range of positions for the swirling vanes.

In addition, the reduced models required a small trace amount of product concentration in order for the reactions to occur. Imposing a minimum floor upon the product species further hampered the models' computational effectiveness.

In contrast, the format of the twelve-specie model fit well into the structure previously developed in AeroSoft's flow and sensitivity solvers. Therefore, we eventually abandoned the reduced global models in favor of a model based on a fundamental reaction mechanism. The drawback of this approach is that the larger number of species significantly added to the computational cost.

3.2   Swirler/Spoke Nozzle Flow

To determine the flow profile at the inlet to the combustion region, we simulate the three-dimensional mixing of air and fuel that takes place in the fuel nozzle. This is a separate up-front calculation where the flow is assumed frozen and turbulent (a two-equation $K-\omega$ model is used). The mass-fraction profiles for N_2, O_2 and CH_4 are then applied as an in-flow profile for the two-dimensional, chemically reacting simulation in the combustor. By running all four swirler-ring cases, we can formulate the sensitivity of the mass-fraction profiles to the swirler location through a Lagrange polynomial. Along with the flow variables, the sensitivity equations can be solved given this mass-fraction sensitivity profile.

Prateep Chatterjee, a doctoral student in the Mechanical Engineering Department at Virginia Tech under the direction of Dr. Uri Vandsburger, has computed the mixing which occurs in the fuel nozzle. Air is introduced at a swirl angle of 45° and mixes with fuel at the spoke ring. Internal mass sources tuned for an equivalence ratio of $\phi = 0.74$ are used to introduce the fuel into the stream. The mass-fraction profiles and axial velocity at the exit of the fuel nozzle are shown in Fig. 2. As the swirling rings are located farther upstream of the combustion region, the swirl ratio decreases at the spoke-ring location. As a result, the mixing in Case 4 is less than in Case 1.

5
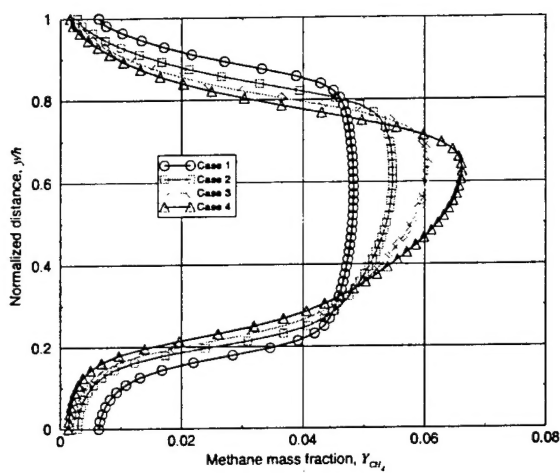
(a) Methane mass-fraction profiles.
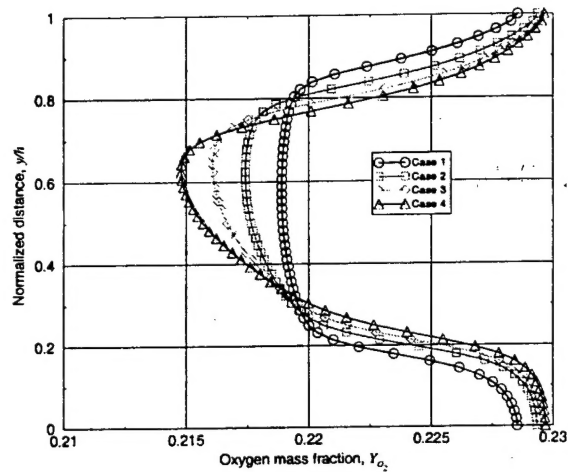
(b) Oxygen mass-fraction profiles.
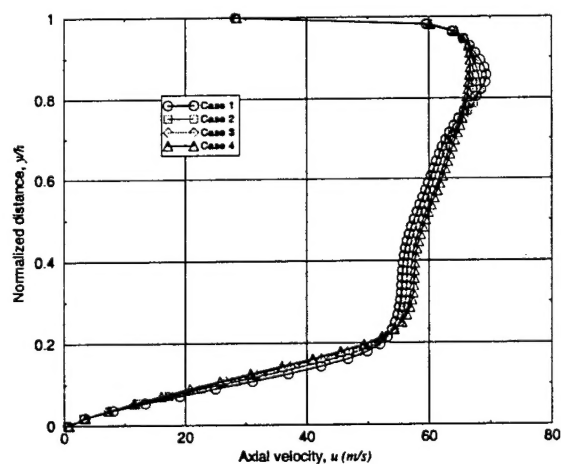
(c) Axial velocity profiles.

Figure 2: Profiles from the axi-symmetric calculations where the swirler location progresses upstream in each of the four cases.

Given the four mass-fraction profiles for specie i at the nozzle exit, the dependency of the local mass fraction upon the swirler-spoke distance (η_s) can be expressed as

$$Y_i(y; \eta_s) = \sum_{j=1}^{4} Y_i^{(j)} \frac{\displaystyle\prod_{\substack{k=1 \\ k \neq j}}^{4} \eta_s - \eta_s^{(k)}}{\displaystyle\prod_{\substack{k=1 \\ k \neq j}}^{4} \eta_s^{(j)} - \eta_s^{(k)}}. \tag{1}$$

The above mass-fraction profile is a cubic function of the swirler distance. Carpet plots of Y_{CH_4} and Y_{O_2} and their sensitivities to η_s are given in Fig. 3. The sensitivity of the profile can be determined by differentiation of the Lagrange polynomial with respect to η_s. The trend discussed above relating decreasing mixing with increasing distance is evident by the negative sensitivity near $y = 0$ and $y = 1$ for $\eta_s = 0.75$ (see Fig. 3(b)). That is, if the swirler-spoke distance increases, then the mass fraction of CH_4 will decrease at the fringes of the mixing layer meaning the fuel has mixed less.

We note that early in the project we proposed to introduce methane via a normal-injection hole. We could then determine the sensitivity of the flow to the hole location by differentiating a continuous flow profile. This idea, while abandoned in the Phase I because it leads to a diffusion flame in the combustor rather than a pre-mixed flame, has produced an AIAA paper which will be presented in January, 2002 [5].

3.3 Combustion-Region Flow

3.3.1 Solution Description

Using AeroSoft's $\mathcal{GASP}$ flow solver, the NETL flow is simulated with third-order spatial accuracy and second-order temporal accuracy. Temporal accuracy is obtained using a dual-time stepping procedure. To take reasonably large physical time steps, the stiff specie production terms (i.e., large in magnitude) must be treated implicitly. Using explicit schemes to solve numerical problems with large source terms requires a very small time step to maintain stability. The implicit procedure in the dual-time stepping method allows us to obtain answers in much fewer time steps. The caveat is that an inner-iteration problem must be converged for each physical time step.

The chemistry model utilizes the methane-air mechanism described in Bowman and Seery's article [4] on shock-induced combustion. The data for the model is given in Table 1. The thermodynamic properties for each of the twelve species are computed using the LeRC curve fits compiled by McBride [6, 7]. By casting the chemical equilibrium problem as a minimization of Gibbs free energy, we can use McBride's data to determine the equilibrium constant and thus, the backward rate.

A number of ideas were utilized to advance the simulation to the steady state. First, we mention two ideas that were not effective.

1. The inlet temperature of the methane/air mixture is too low ($T_i = 583\,K$) to ignite. Furthermore, sources for combustion do not exist anywhere in the flow field (e.g., a hot wall or shock-induced combustion). A heat source is necessary to ignite the flow, yet none exists physically. The result is a cold-flow calculation.
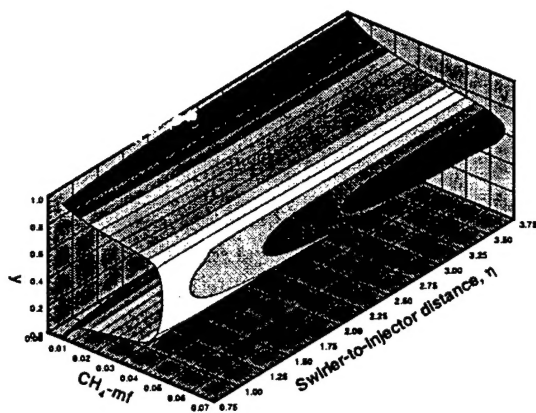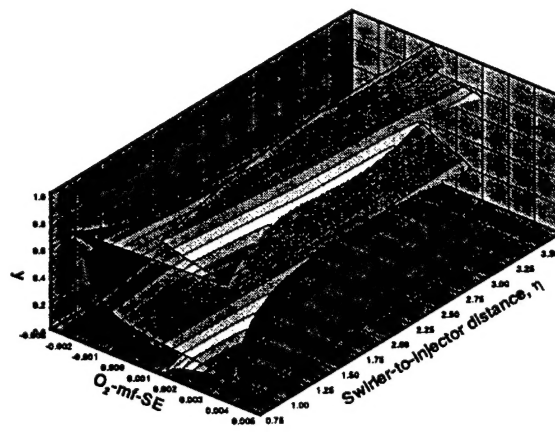
(a) Methane mass fraction, $Y_{CH_4}(y; \eta_s)$.
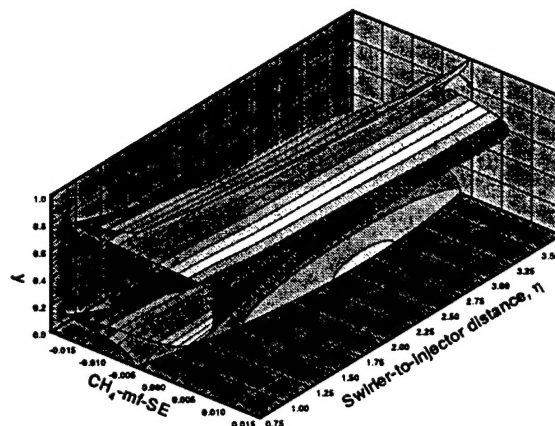
(b) Methane sensitivity, $\partial Y_{CH_4}/\partial \eta_s$.
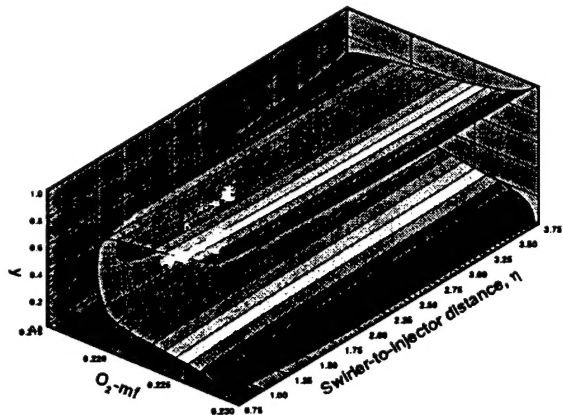
(c) Oxygen mass fraction, $Y_{O_2}(y; \eta_s)$.

(d) Oxygen sensitivity, $\partial Y_{O_2}/\partial \eta_s$.

Figure 3: The mass fraction profiles and sensitivities in (y, η_s) space.

j	Reaction	$k_f = AT^\eta \exp(-E_a/T)$		
		A	η	E_a
1	$CH_4 + M \rightleftharpoons CH_3 + H + M$	2.0×10^{17}	0.0	44,500
2	$CH_4 + OH \rightleftharpoons CH_3 + H_2O$	2.8×10^{13}	0.0	2,500
3	$CH_4 + O \rightleftharpoons CH_3 + OH$	2.0×10^{13}	0.0	4,640
4	$CH_4 + H \rightleftharpoons CH_3 + H_2$	6.9×10^{13}	0.0	5,950
5	$CH_3 + O_2 \rightleftharpoons HCO + H_2O$	2.0×10^{10}	0.0	0
6	$CH_3 + O \rightleftharpoons HCO + H_2$	1.0×10^{14}	0.0	0
7	$HCO + OH \rightleftharpoons CO + H_2O$	1.0×10^{14}	0.0	0
8	$HCO + M \rightleftharpoons H + CO + M$	2.0×10^{12}	0.5	14,400
9	$CO + OH \rightleftharpoons CO_2 + H$	5.6×10^{11}	0.0	545
10	$H + O_2 \rightleftharpoons O + OH$	2.2×10^{14}	0.0	8,340
11	$O + H_2 \rightleftharpoons H + OH$	1.7×10^{13}	0.0	4,750
12	$O + H_2O \rightleftharpoons 2OH$	5.8×10^{13}	0.0	9,070
13	$H + H_2O \rightleftharpoons H_2 + OH$	8.4×10^{13}	0.0	10,100
14	$H + OH + M \rightleftharpoons H_2O + M$	1.0×10^{19}	-1.0	0

Table 1: Methane-Oxygen reaction mechanism utilized in the NETL combustion region (from Bowman and Seery [4]). Collision efficiencies cited from Warnatz [8] are $M = H_2$ [1.0], O_2 [0.4], N_2 [0.4], H_2O [6.5], CO [0.75], CO_2 [1.5], CH_4 [6.5]. Note: N_2 is an inert specie.

2. Raising the static temperature artificially by manipulating the specie densities at certain strategic spots in the flow results in local "explosions". The local velocity pattern is corrupted significantly and the local Mach number increases unrealistically. After disabling the temperature source, the flow field does not regain a realizable pattern and the approach is abandoned.

To obtain the correct flow pattern, we must work backwards beginning with the primary products rather than the reactants. The flow is assumed to consist only of N_2, CO_2, and H_2O at a high temperature, $T = 1500\,K$. Once this frozen flow calculation has converged, we convert the solution to the 12-specie finite-rate chemistry model. We then impose the inlet conditions as a boundary condition using the hot-flow solution as an initial restart.

The inlet conditions for the nozzle correspond to data provided by Douglas Straub of the National Energy Technology Laboratory. The equivalence ratio, nozzle velocity, and inlet temperature are $\phi = 0.74$, $U_i = 55.6\,m/s$ and $T_i = 583\,K$. The total pressure in the plenum is $p_0 = 7.5\,atm$, and this results in an inlet Mach number of $M_i = 0.1172$. Once the flow with these uniform inlet conditions becomes pseudo-steady, we apply the profile from the axi-symmetric mixing calculations discussed in Sec. 3.2. Flow visualization of the temperature, Mach number, and reactants are shown in Fig. 4.
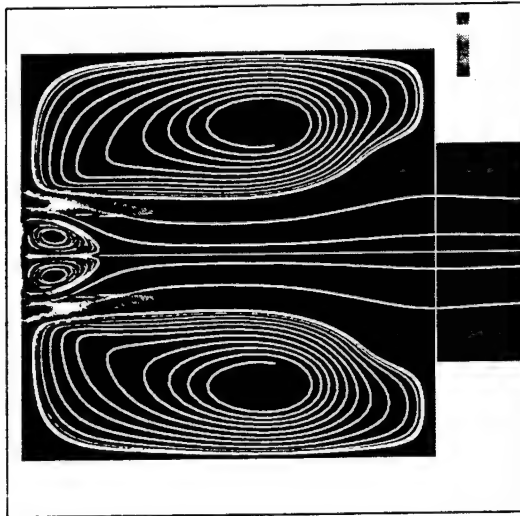
The flow consists of a planar pre-mixed jet which generates two counter-rotating vortices – one at the base region of the combustor and the other upstream of the constrictor plug. The vortices squeeze the flame which is completely burned approximately 2.6" into the combustor.
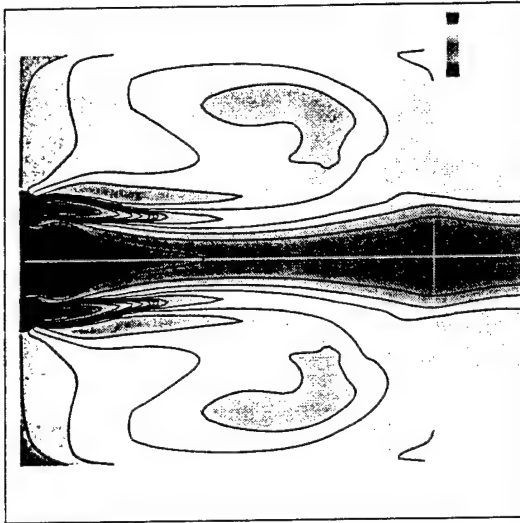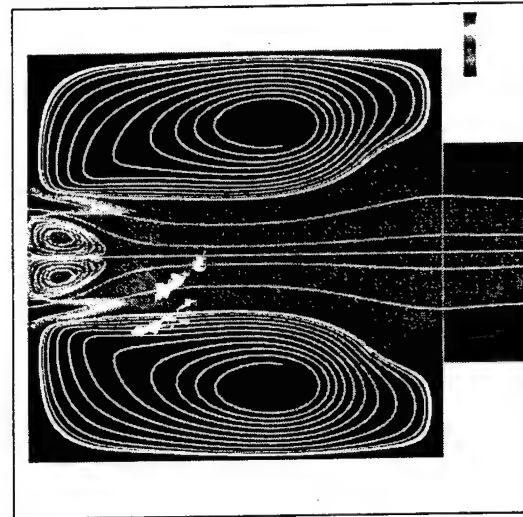
(a) Temperature, T.
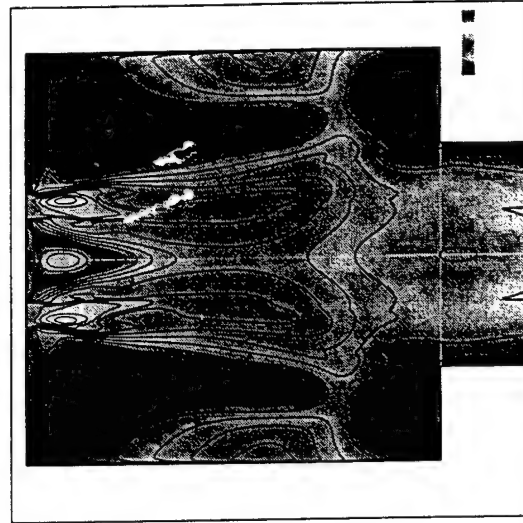
(b) Mach number, M.

(c) Methane mass fraction, Y_{CH_4}.

(d) Oxygen mass fraction, Y_{O_2}.

Figure 4: Flow visualization of the steady flow solution.

3.3.2 Integral Sensitivity Equations

The integral form of the time-dependent sensitivity equations can be written as follows.

$$\frac{\partial}{\partial t} \iiint \mathbf{S}\, dV + \oint_A \mathbf{F}'(\mathbf{S}; \mathbf{Q}) \cdot \hat{n}\, dA = \oint_A \mathbf{F}'_v(\mathbf{S}; \mathbf{Q}) \cdot \hat{n}\, dA + \iiint \mathbf{W}'\, dV \qquad (2)$$

The flow sensitivity is denoted as $\mathbf{S}$ and is defined as $\partial \mathbf{Q}/\partial \eta$. $\mathbf{Q}$ represents the vector of conserved variables and η is a generic design variable. The sensitivity of the inviscid and viscous flux vectors are denoted as $\mathbf{F}'$ and $\mathbf{F}'_v$, respectively. The change of chemical composition by combustion is controlled by the source term, $\mathbf{W}$. Before the sensitivities can be determined, the flow variables must be known in the form of $\mathbf{Q}$. In our "snap-shot" sensitivities, we solve the steady-state version of Eqn. (2).

3.4 Unsteady Flow History

In the NETL experiments, a lean mixture of fuel/air burns on the edge of being extinguished in the combustor. As a result, pressure waves oscillate from the combustion region and affect the mass flow of air ($\dot{m}_{air}$) entering the nozzle from the plenum. (Note: the mass flow of fuel is choked and, thus, fixed in time.) The changing mass flow generates a time-dependent equivalence ratio at the flame front. As this mixture burns, the pressure waves increase in amplitude until the oscillations resonate at the vibrational modes of the system. If this process continues, the combustor can be damaged. The key component that we focus upon is that the aero-acoustic instability causes the mass flow of air to be unsteady.

In our investigation, we separate the effects of the aero-acoustic instability by analyzing a forced unsteadiness at the inlet to the combustor. In particular, by making the mass fraction profiles a function of time we can vary the equivalence ratio without affecting mass flow. Likewise, we can change the flow velocity without changing the equivalence ratio. Finally, we can change the density profiles and change both simultaneously. By denoting the baseline properties with a 0 superscript, we can summarize the cases as follows.

- Variable mass flow, Fixed equivalence ratio.

$$
\begin{aligned}
\rho_{N_2} &= \rho^0\, Y_{N_2}^0(y; \eta_s) \\
\rho_{O_2} &= \rho^0\, Y_{O_2}^0(y; \eta_s) \\
\rho_{CH_2} &= \rho^0\, Y_{CH_2}^0(y; \eta_s) \\
u &= u^0(y; \eta_s)\left[1 + \epsilon \sin(\omega t)\right]
\end{aligned}
$$

- Fixed mass flow, Variable equivalence ratio.

$$
\begin{aligned}
\rho_{N_2} &= \rho^0\, Y_{N_2}^0(y; \eta_s)[1 + \epsilon \sin(\omega t)] \\
\rho_{O_2} &= \rho^0\, Y_{O_2}^0(y; \eta_s)[1 + \epsilon \sin(\omega t)] \\
\rho_{CH_2} &= \rho^0 - \rho_{N_2} - \rho_{O_2} \\
u &= u^0(y; \eta_s)
\end{aligned}
$$

- Variable mass flow, Variable equivalence ratio.

$$
\begin{aligned}
\rho_{N_2} &= \rho^0 Y_{N_2}^0(y; \eta_s)[1 + \epsilon \sin(\omega t)] \\
\rho_{O_2} &= \rho^0 Y_{O_2}^0(y; \eta_s)[1 + \epsilon \sin(\omega t)] \\
\rho_{CH_2} &= \rho^0 Y_{CH_2}^0(y; \eta_s) \\
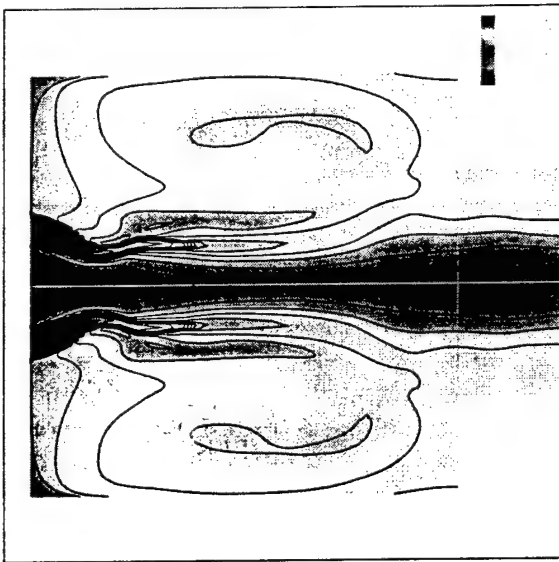u &= u^0(y; \eta_s)
\end{aligned}
$$

In our case, the baseline mixture density is constant for all $(y; \eta_s)$ combinations and equals $\rho^0 = 4.761 \, kg/m^3$. For an equivalence ratio of $\phi = 0.74$, the mass fractions are $Y_{N_2} = 0.7353$, $Y_{O_2} = 0.2233$ and $Y_{CH_4} = 0.0414$. The sinusoidal oscillation is specified according to the experimentally observed fluctuations in pressure. A 6.93% change in the amplitude corresponds to $\epsilon = 0.0693$ and the measured frequency is $\omega = 237 \, Hz$. Four snap-shots of the temperature are shown in Fig. 5. The methane mass-fraction contours are given in Fig. 6. The flame bends toward the centerline over time, but at a much lower frequency than the forced inflow oscillation.

3.4.1 Snapshot Sensitivities

For the three forced instabilities discussed earlier, the sensitivity profile is determined by differentiation with respect to η_s. The resulting profiles are given below.

- Variable mass flow, Fixed equivalence ratio.

$$
\begin{aligned}
\rho_{N_2}' &= \rho^0 [Y_{N_2}^0]'(y; \eta_s) \\
\rho_{O_2}' &= \rho^0 [Y_{O_2}^0]'(y; \eta_s) \\
\rho_{CH_2}' &= \rho^0 [Y_{CH_2}^0]'(y; \eta_s) \\
u' &= 0
\end{aligned}
$$

- Fixed mass flow, Variable equivalence ratio.

$$
\begin{aligned}
\rho_{N_2}' &= \rho^0 [Y_{N_2}^0]'(y; \eta_s)[1 + \epsilon \sin(\omega t)] \\
\rho_{O_2}' &= \rho^0 [Y_{O_2}^0]'(y; \eta_s)[1 + \epsilon \sin(\omega t)] \\
\rho_{CH_2}' &= -\rho_{N_2}' - \rho_{O_2}' \\
u' &= 0
\end{aligned}
$$

- Variable mass flow, Variable equivalence ratio.

$$
\begin{aligned}
\rho_{N_2}' &= \rho^0 [Y_{N_2}^0]'(y; \eta_s)[1 + \epsilon \sin(\omega t)] \\
\rho_{O_2}' &= \rho^0 [Y_{O_2}^0]'(y; \eta_s)[1 + \epsilon \sin(\omega t)] \\
\rho_{CH_2}' &= \rho^0 [Y_{CH_2}^0]'(y; \eta_s) \\
u &= 0
\end{aligned}
$$

During the Phase I, we investigate only the first case where the mass flow is variable but the equivalence ratio remains constant.
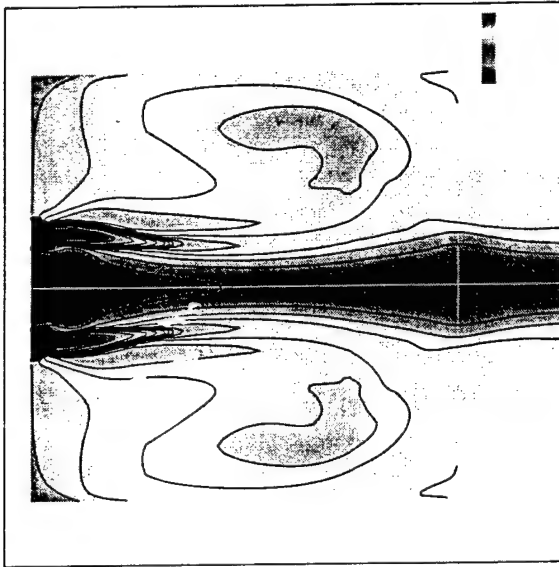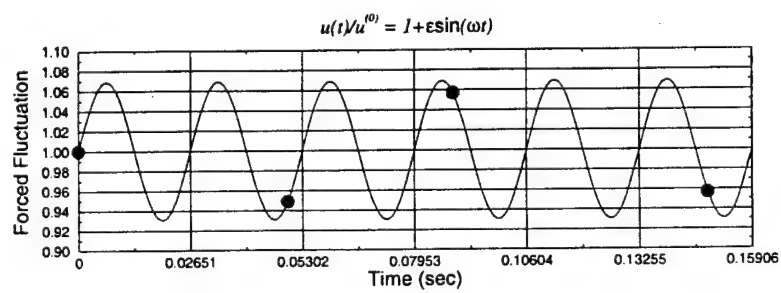
(a) Time, $t = 0.0000\,sec.$
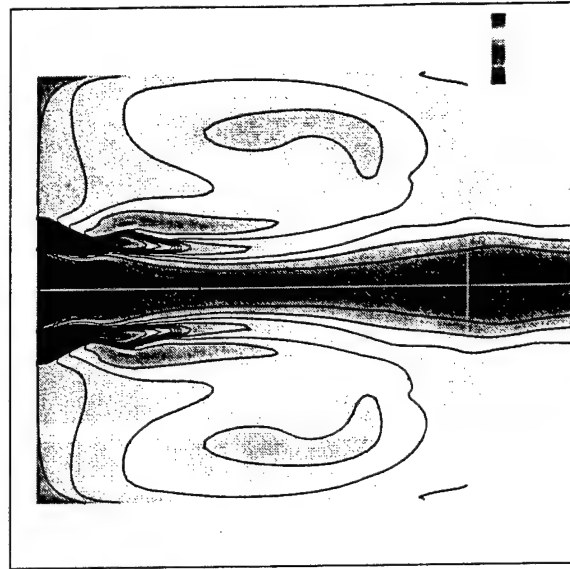
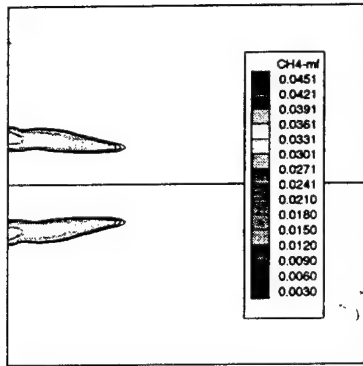(b) Time, $t = 0.0494\,sec.$

(c) Time, $t = 0.0888\,sec.$

(d) Time, $t = 0.1480\,sec.$

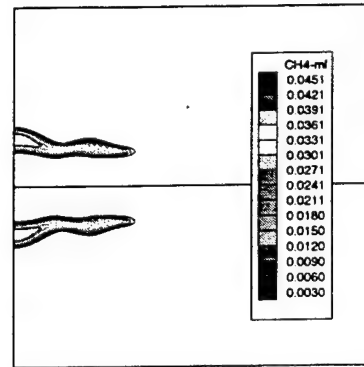$$u(t)/u^{(0)} = 1 + \varepsilon\sin(\omega t)$$
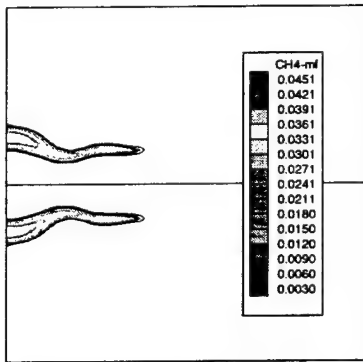
(e) Boundary condition history.

13
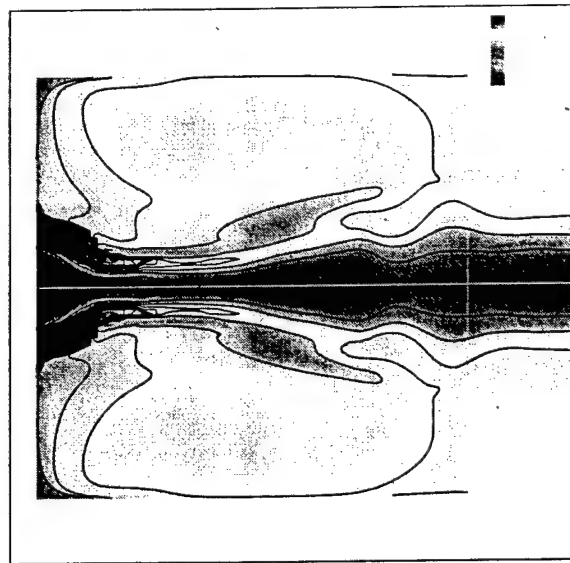
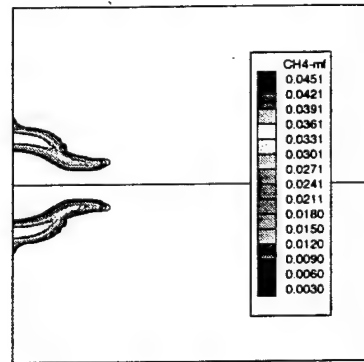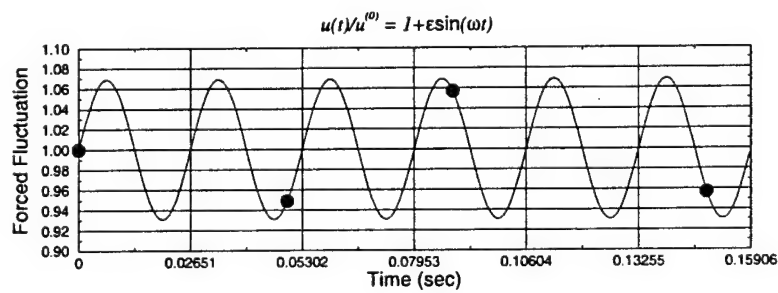Figure 5: Unsteady temperature contours, T.

(a) Time, $t = 0.0000\,sec.$

(b) Time, $t = 0.0494\,sec.$

(c) Time, $t = 0.0888\,sec.$

(d) Time, $t = 0.1480\,sec.$

(e) Boundary condition history.
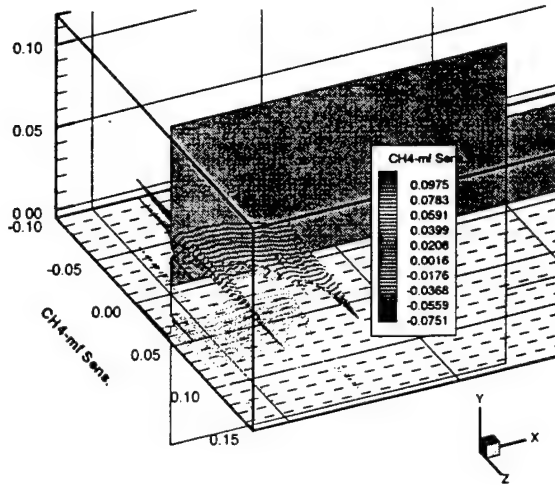
Figure 6: Unsteady methane mass-fraction contours, Y_{CH_4}.

1. Sensitivity to inlet velocity, $\eta = U_i$.

   Fig. 7 shows the snap-shot sensitivities to the inlet velocity. One would reason for a fixed flame speed, increasing the inlet velocity would move the flame front farther into the combustion region. This would be indicated by a positive sensitivity in the methane mass fraction aft of the flame front. Fig. 7(a) indicates a trend which moves the flame.

2. Sensitivity to swirler location, $\eta = \eta_s$.

   Fig. 8 depicts the mass-fraction sensitivity to increasing the swirler distance (i.e., moving the swirler farther upstream of the combustion region). For all time levels, we see the effects of decreased mixing in the sensitivity plots. We see that methane mass-fraction at the core of the mixture increases with increasing distance. The effect is more pronounced at the last time level studied than at the first.

   Fig. 9 shows pressure-sensitivity contours with increasing swirler distance. from these plots we notice that "pockets" of pressure fluctuation exist near the flame front as the swirler is moved. The pressure away from the flame seems to be relatively unaffected by a new swirler location.
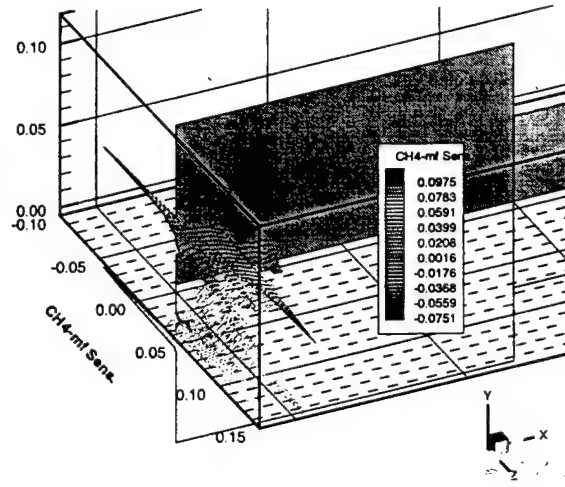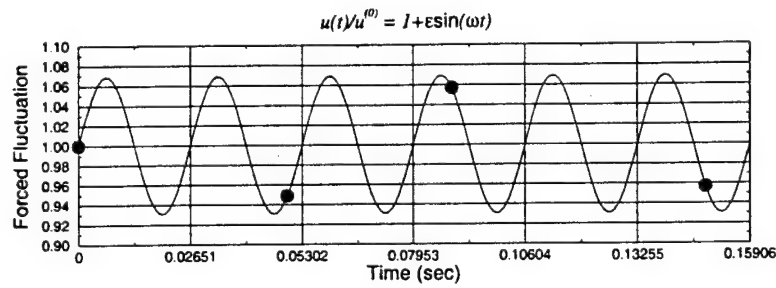
(a) Time, $t = 0.0000\,sec.$

(b) Time, $t = 0.0494\,sec.$
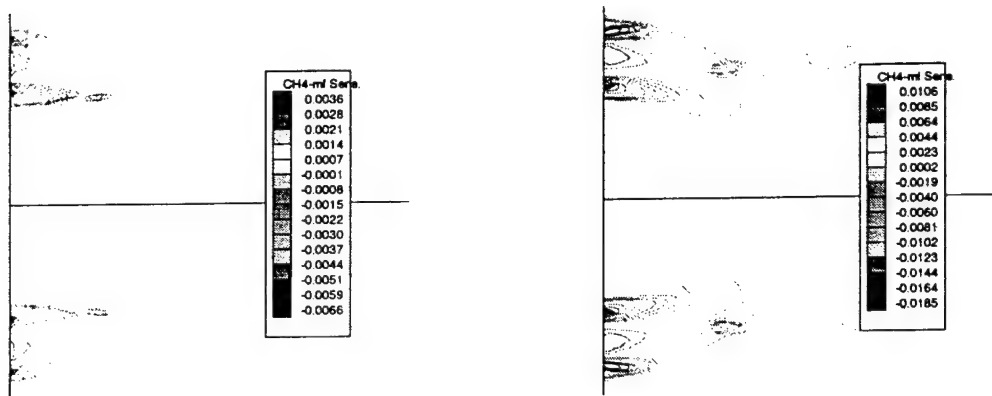
(c) Time, $t = 0.0888\,sec.$

(d) Time, $t = 0.1480\,sec.$

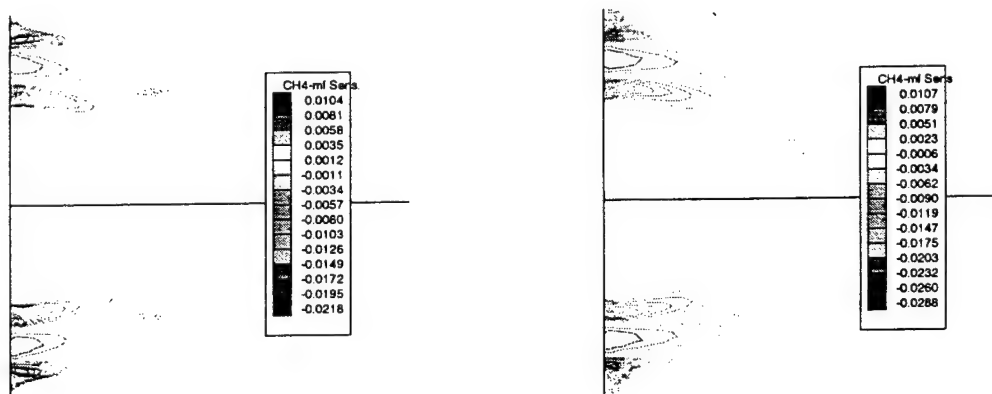$u(t)/u^{(0)} = 1 + \varepsilon\sin(\omega t)$
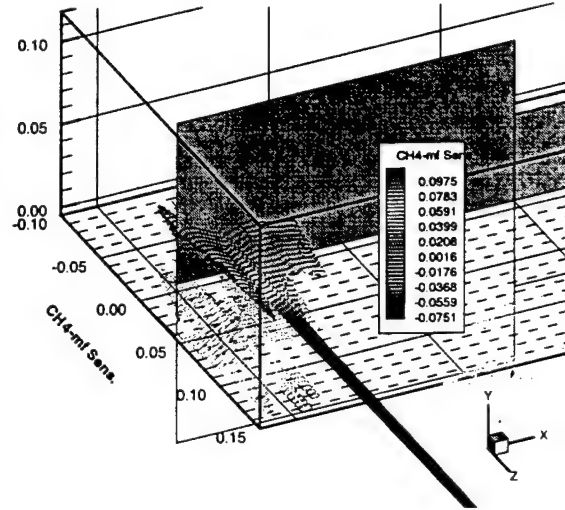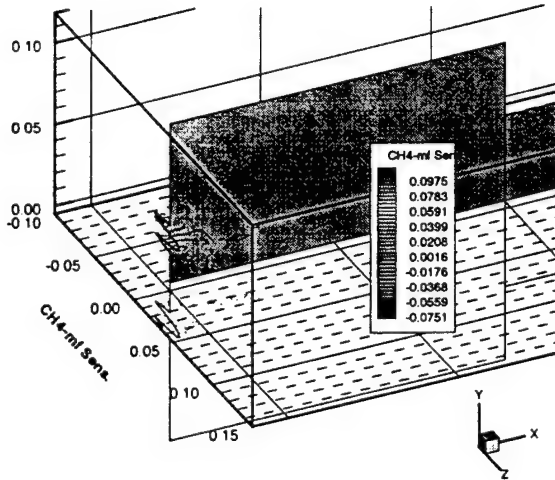
(e) Boundary condition history.

Figure 7: Contours of unsteady methane mass-fraction sensitivity to inlet velocity, Y'_{CH_4}, $\eta = U_i$.

16
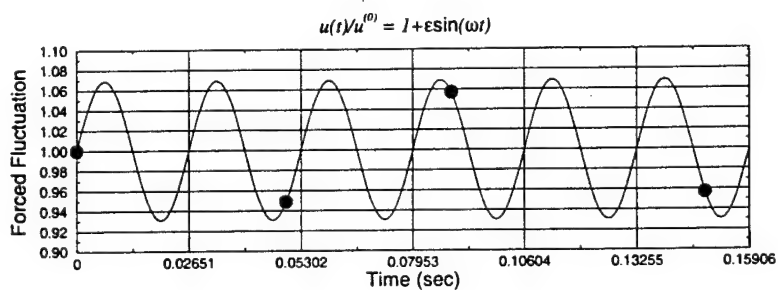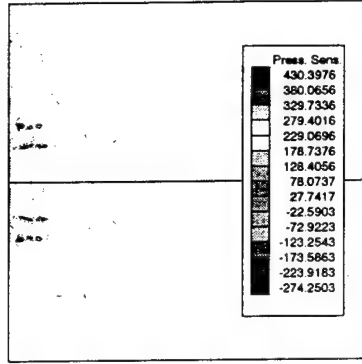
(a) Time, $t = 0.0000\,sec.$

(b) Time, $t = 0.0494\,sec.$

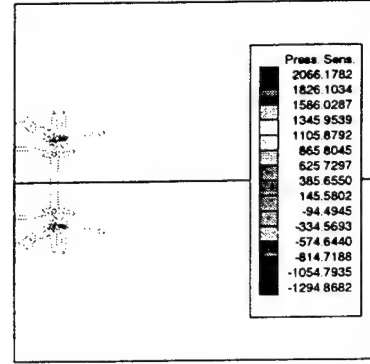(c) Time, $t = 0.0888\,sec.$

(d) Time, $t = 0.1480\,sec.$

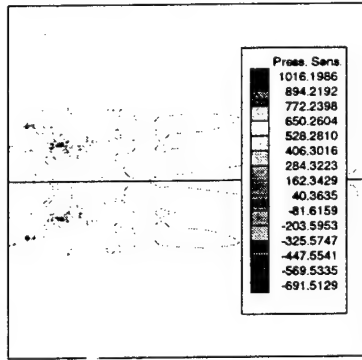(e) Boundary condition history.

Figure 8: Contours of unsteady methane mass-fraction sensitivity to swirler location, Y'_{CH_4}, $\eta = \eta_s$.
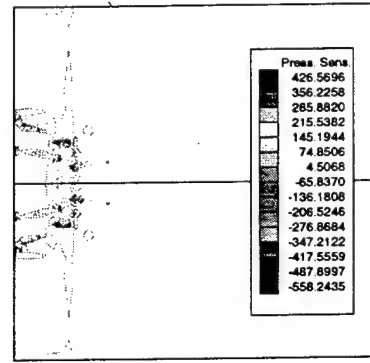
17

(a) Time, $t = 0.0000\,sec.$
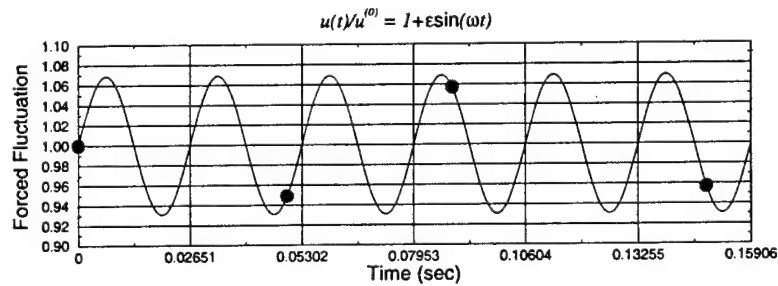
(b) Time, $t = 0.0494\,sec.$

(c) Time, $t = 0.0888\,sec.$

(d) Time, $t = 0.1480\,sec.$

(e) Boundary condition history.

Figure 9: Contours of unsteady pressure sensitivity to swirler location, p', $\eta = \eta_s$.

18

3.5 1-D, Unsteady Sensitivity Solutions

The above snap-shot sensitivities do not incorporate sensitivity history like a true time-dependent sensitivity solution. To compute real unsteady sensitivities, we must solve the sensitivity equations immediately after taking a physical time step in the flow. In other words, we must solve the flow/sensitivity equations as a coupled set. We test the coupled solver by solving several test problems. The first is an example which compares well with previously published results by Appel and Gunzburger [9]. The remaining examples demonstrate sensitivity with respect to (a) the initial density (with a uniform heat source), (b) a Bezier parameter which describes the shape of the nozzle cross-sectional area.

3.5.1 10:1 Riemann Problem

To verify our solution procedure, we solve a Riemann problem proposed by Sod [10]. The unsteady sensitivity to the high-pressure is computed simultaneously. For this example, we consider a constant area duct of unit length $x \in (0,1)$ with initial conditions stated in terms of density, velocity and pressure as

$$\left\{ \begin{array}{c} \rho \\ u \\ p \end{array} \right\}_L = \left\{ \begin{array}{c} 1 \\ 0 \\ 1 \end{array} \right\}, \qquad \left\{ \begin{array}{c} \rho \\ u \\ p \end{array} \right\}_R = \left\{ \begin{array}{c} 0.125 \\ 0 \\ 0.1 \end{array} \right\}, \tag{3}$$

The initial flow is separated by a "diaphragm" located at $x = 0.5$, and the initial value problem solved with 100 cells of uniform width. All initial sensitivities are uniformly zero, except $p_L = 1.0$. Results at $t = 0.142$ with a time step of $\Delta t = 10^{-3}$ are given in Fig. 10 and Fig. 11. Note that the sensitivities compare well with central difference solutions with a step size of $\Delta p = 0.001$ (see Figure 12). The noticeable discrepancies occur at the locations of singularities in the true solution.

3.5.2 1-D Nozzle Sensitivities

In this problem, we consider a linearly expanding nozzle with constant initial data as given below.

$$\rho(0, x) = 1.2256, \qquad \rho u(0, x) = 833.65, \qquad \rho e_0(0, x) = 5.3667 \times 10^5$$

We consider the sensitivity of the evolving flow to the inlet density with a uniform heat source. The idea behind the heat source is to generalize the specie production in the 1-D case. The results at $t = 0.142 \, sec$ are given in Fig. 13. If we specify the shape of the nozzle using a Bezier curve, we can determine the sensitivity to a control point. The results for this problem are given in Fig. 14.

4 Potential Use by the Federal Government

The most immediate use within government-sponsored programs is within the field of unsteady flow control. The instantaneous sensitivity can be used to modify flow features advantageously. Immediate applications could be dynamic flutter analysis, tactical missile propulsion and control, and high-performance aircraft maneuverability.
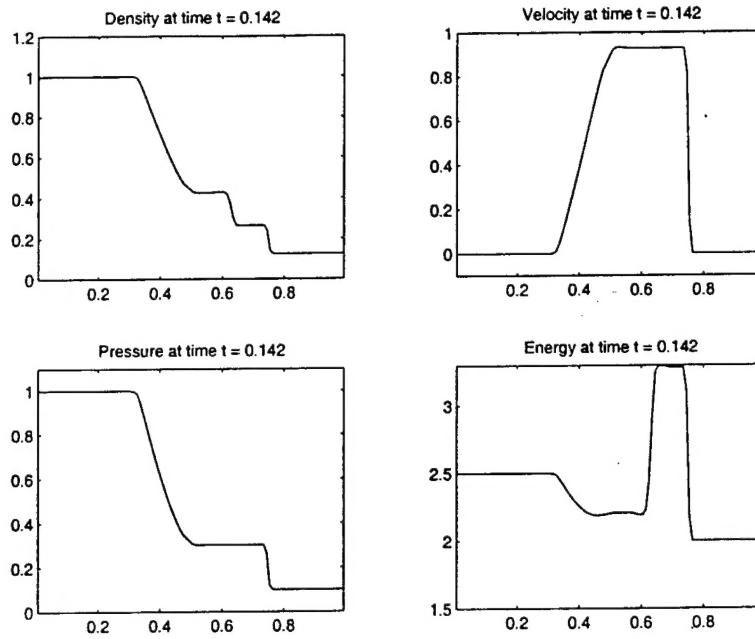
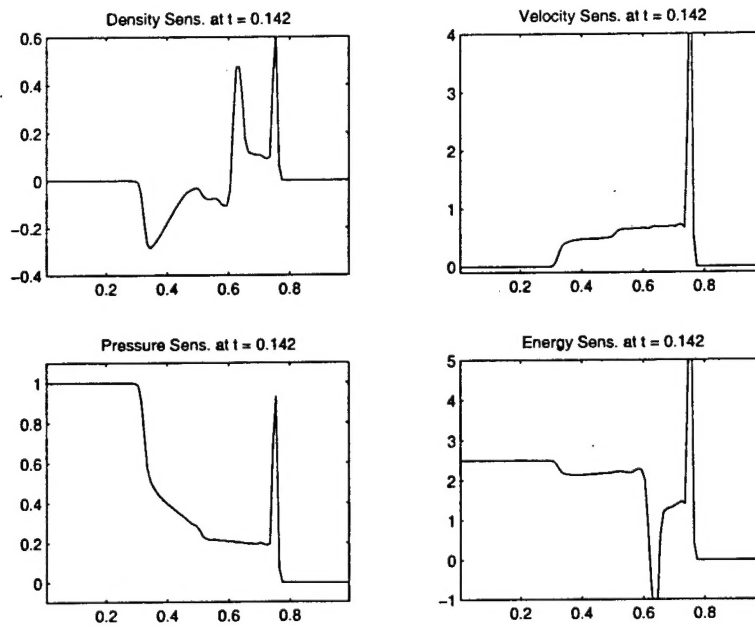19

Figure 10: Riemann Problem, Flow Variables

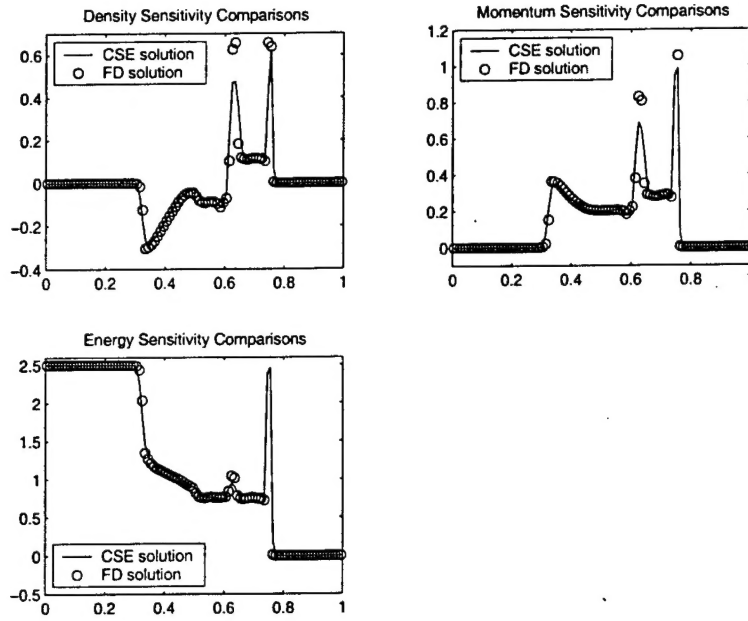Figure 11: Riemann Problem, Sensitivity Variables

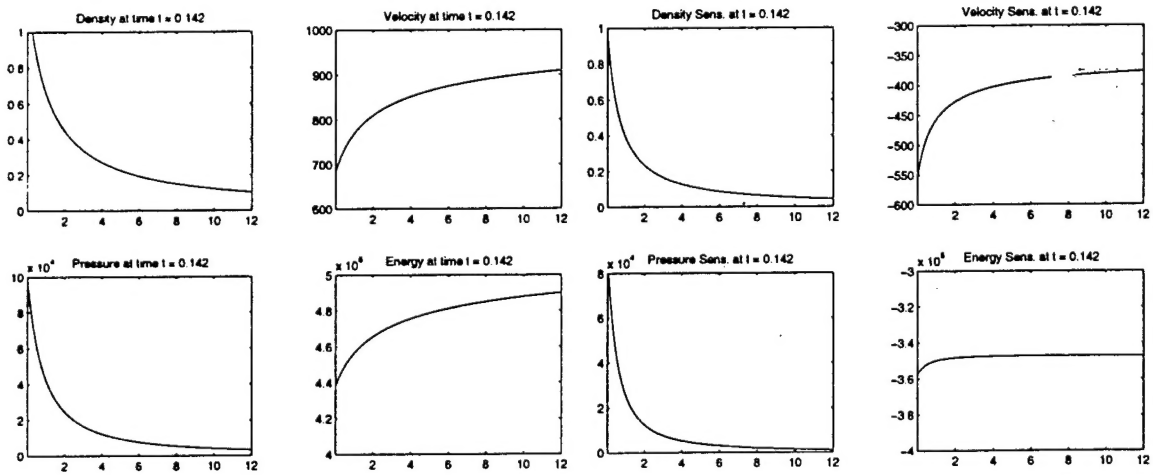Figure 12: Comparison of CSE with Central Differences

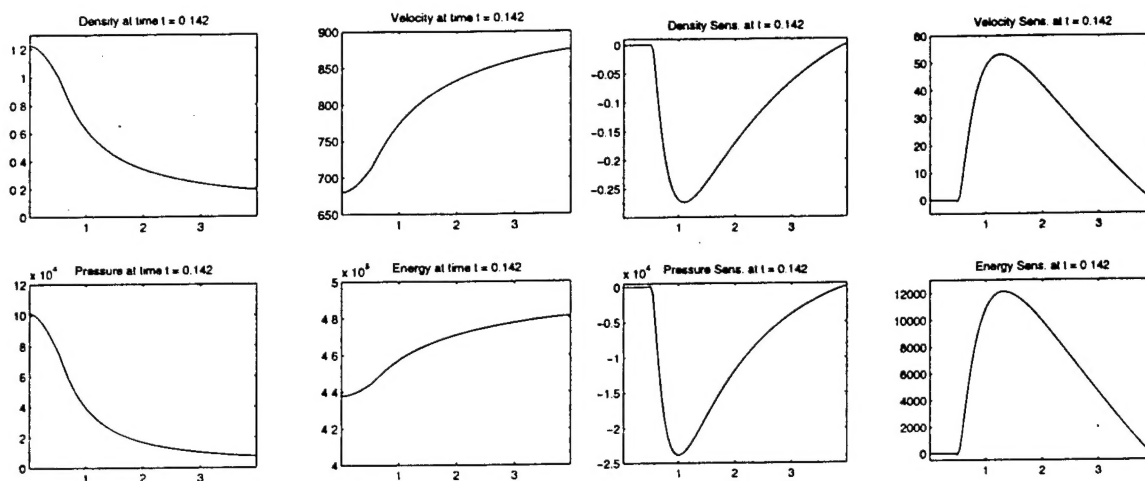Figure 13: Flow and Sensitivity Solutions for Initial Density Sensitivity.

Figure 14: Flow and Sensitivity Solutions for Bezier Parameter Sensitivity.

References

[1] C. K. Woodbrook and F. L. Dryer. "Simplified Reaction Mechanisms for the Oxidation of Hydrocarbon Fuels in Flames". *Combustion Science and Technology*, **27**:31–43, 1981.

[2] N. Peters and R. J. Kee. "The Computation of Stretched Laminar Methane-Air Diffusion Flames Using a Reduced Four-Step Mechanism". *Combustion and Flame*, **68**:17–29, 1987.

[3] G. Paczko, P. M. Lefdal, and N. Peters. "Reduced Reaction Schemes for Methane, Methanol and Propane Flames". Technical report, 21st *International Symposium on Combustion/The Combustion Institute*, 1996.

[4] C. T. Bowman and D. J. Seery. "Investigation of NO Formation Kinetics in Combustion Processes: The Methane-Oxygen-Nitrogen Reaction". In W. Cornelius and W. G. Agnew, editors, **Emissions for Continuous Combustion Systems**, pages 123–139. Plenum Press, 1972. Symposium on Emissions from Continuous Combustion Systems held at the General Motors Research Laboratories, Warren, Michigan, September 27-28, 1971.

[5] J. T. Borggaard, E. M. Cliff, and A. G. Godfrey. "Sensitivity Analysis with Sliding Boundary Conditions". AIAA Paper 02-0100, 40th *AIAA Aerospace Sciences Meeting and Exhibit*, January 14-17 2002.

[6] B. J. McBride, S. Gordon, and M. A. Reno. "Thermodynamic Data for Fifty Reference Elements". NASA TP-3287, National Aeronautics and Space Administration, January 1993.

[7] B. J. McBride, S. Gordon, and M. A. Reno. "Coefficients for Calculating Thermodynamic and Transport Properties of Individual Species". NASA TM-4513, National Aeronautics and Space Administration, October 1993.

[8] J. Warnatz. "Rate Coefficients in the C/H/O System". In W. C. Gardiner Jr., editor, **Combustion Chemistry**, chapter 5, pages 197–360. Springer-Verlag, 1982.

[9] J. R. Appel and M. D. Gunzburger. "Difficulties in Sensitivity Calculations for Flow with Discontinuities". *AIAA Journal*, **35**(5):842–848, 1997.

[10] G. A. Sod. "A Survey of Several Finite-Difference Methods for Systems of Non-linear Hyperbolic Conservation Laws". *Journal of Computational Physics*, **27**:1–31, 1978.